Multiple recent sex chromosome fusions in *Drosophila virilis* associated with elevated satellite DNA abundance

Jullien M. Flynn*, Kevin B. Hu, Andrew G. Clark

Department of Molecular Biology and Genetics, Cornell University, Ithaca, NY

*Corresponding author: jmf422@cornell.edu

ABSTRACT

Repetitive satellite DNA is highly variable both within and between species, and is often located near centromeres. However, the abundance or array length of satellite DNA may be constrained or have maximum limits. *Drosophila virilis* contains among the highest relative satellite abundances, with almost half its genome composed of three related 7 bp satellites. We discovered a strain of *D. virilis* that has 15% more pericentromeric satellite DNA compared to other strains, and also underwent two independent centromere-to-centromere sex chromosome fusion events. These fusions are presumably caused by DNA breakage near the pericentromeric satellites followed by repair using similar repetitive regions of nonhomologous chromosomes. We hypothesized that excess satellite DNA might increase the risk of DNA breaks and genome instability when stressed, which would be consistent with the apparent high rate of fusions we found in this strain. To directly quantify DNA breakage levels between strains with different satellite DNA abundances, we performed the comet assay after feeding flies gemcitabine and administering low-dose gamma radiation. We found a positive correlation between the rate of DNA breakage and satellite DNA abundance. This was further supported by a significant decrease in DNA breakage in an otherwise genetically identical substrain that lost the chromosome fusion and several megabases of satellite DNA. We find that the centromere-to-centromere fusions resulted in up to a 21% nondisjunction rate between the X and Y chromosomes in males, adding a fitness cost. Finally, we propose a model consistent with our

30 data that implicates genome instability as a critical evolutionary constraint to satellite
31 abundance.
32

33
34 **INTRODUCTION**
35
36 Satellite DNA consists of long arrays of tandemly repeated sequences, and is often located near
37 centromeres in heterochromatin (reviewed in Thakur *et al.* 2021). Satellite DNA varies greatly in
38 sequence and abundance within and between species (Subirana *et al.* 2015; Wei *et al.* 2018;
39 Cechova *et al.* 2019), and this can be partially explained by high rates of copy number mutation
40 (Flynn *et al.* 2017). Although previously assumed to be inert "junk," recent work has shown that
41 satellite DNA is involved in essential processes in the cell, thus variation in it may be biologically
42 important (Jagannathan *et al.* 2018; Mills *et al.* 2019). Although satellite DNA differences
43 between some species have been linked to reproductive incompatibilities (Ferree and Barbash
44 2009; Jagannathan and Yamashita 2021), the biological implications of intraspecies abundance
45 variation has not been explored. Satellite DNA can vary in abundance by several megabases
46 among individuals of the same species, including in flies and humans (Miga *et al.* 2014; Wei *et*
47 *al.* 2014; Flynn *et al.* 2020). Satellite DNA appears to be constrained by maximum limits, with no
48 species studied so far having more than about half of their genome made up of satellite DNA
49 (Gall and Atherton 1974a; Fry and Salser 1977; Petitpierre *et al.* 1995). The genomic abundance
50 of transposable elements (TEs), the other highly pervasive type of repetitive DNA, seems to be
51 less constrained than satellite DNA with many genomes over 50% and some containing up to
52 85% TE content (Anderson *et al.* 2019). The nature of satellite DNA with long tandem arrays of
53 the same sequence, may impose instability that prevents it from expanding beyond a threshold,
54 compared to more diverse sequences interspersed in the genome.
55
56 *Drosophila virilis* is an excellent model for studying satellite DNA variation. *D. virilis* has the
57 highest relative abundance of simple satellite DNA (defined as satellites with unit length <=20
58 bp) compared to any other studied species. Three 7 bp satellites, AAACTAC, AAACTAT, and
59 AAATTAC take up over 40% of the genome in *D. virilis*, and they form arrays tens of megabases
60 long in the pericentromeric region (Gall *et al.* 1971; Gall and Atherton 1974; Flynn *et al.* 2020).
61 The extremely high relative abundance of satellite DNA in *D. virilis* makes it an ideal system in
62 which to ask whether there are constraints or maximum limits on satellite abundance. One

63 strain in particular, vir00 (15010-1051.00), contains 15% more pericentromeric satellite DNA
64 compared to other *D. virilis* strains (Flynn *et al.* 2020 Figure 4B). In past modeling efforts,
65 satellite DNA arrays have been proposed to be weakly deleterious until they reach a maximum
66 length beyond which they are not tolerated by selection (Charlesworth *et al.* 1986). Slow DNA
67 replication or development time have been suggested as mechanisms to enforce strong
68 negative selection against long satellite arrays, however empirical evidence for this has been
69 limited (but see Bilinski *et al.* 2018). Here, we propose genome instability as a constraint on
70 excessively long or abundant satellite DNA arrays.
71
72 Genome instability is characterized by DNA damage that often results in large-scale mutations
73 or rearrangements, and is a fundamental driver of karyotype evolution, chromosomal
74 disorders, and cancer rearrangements (Black and Giunta 2018; Mayrose and Lysak 2021). The
75 first step is spontaneous DNA damage such as double-stranded DNA breaks, one of the most
76 dire events to occur in a cell (Featherstone and Jackson 1999). Even if DNA breaks are repaired,
77 they often result in large-scale genome rearrangements. Most DNA breaks leading to
78 rearrangements occur near the centromere and within or near satellite DNA, including in
79 human genomes (Black and Giunta 2018; Balzano *et al.* 2020). This may be due to intrinsic
80 instability of satellite DNA arrays caused by replication stress of polymerases progressing
81 through highly repetitive sequences, or the formation of unstable DNA topology (Barra and
82 Fachinetti 2018). Robertsonian translocations, one of the most common rearrangements in
83 medical genetics and evolution, occur when there are breaks near the centromere of
84 acrocentric chromosomes and when they are repaired they are fused to each other (Mayrose
85 and Lysak 2021). Robertsonian translocations are associated with multiple miscarriages in
86 humans and aneuploidy disorders like Patau and Down syndromes (Braekeleer and Dao 1990),
87 with increased rates of aneuploidy driven by increased nondisjunction of Robertsonian or fused
88 chromosomes (Schulz *et al.* 2006). We hypothesize that variation in pericentromeric satellite
89 DNA abundance influences the risk of genome instability events. Specifically, excess satellite
90 DNA might increase the risk of genome instability and genome rearrangements.
91

92 Sex chromosome evolution has been studied for decades, mainly making use of sex
93 chromosomes that have arisen in different time periods (Charlesworth and Charlesworth 2000).
94 In Drosophila, when an autosome fuses to either an X or Y chromosome, a so-called neo-Y
95 chromosome is formed. Because either the fused or unfused version of the chromosome will
96 only be present in males and male Drosophila do not undergo recombination, mutations
97 immediately begin to accumulate through Hill-Robertson interference and other linked-
98 selection processes (Charlesworth and Charlesworth 2000). In the genus Drosophila, autosomes
99 have fused to sex chromosomes multiple independent times (Nozawa *et al.* 2021): *D.*
100 *pseudoobscura* (10 million years), *D. miranda* (1 million years; Bachtrog 2013), *D. albomicans*
101 (0.24 million years; (Wei and Bachtrog), and *D. americana* (29 thousand years; (Vieira *et al.*
102 2006). Neo-sex chromosomes formed by *de novo* sex chromosome fusions are rare and actually
103 under-represented compared to autosomal fusions in *Drosophila* (Anderson *et al.* 2020), and
104 have never been discovered at their infancy before detectable divergence has occurred. How
105 new sex chromosome fusions become stable, and how they compete with the ancestral
106 karyotype within a species is unknown.
107
108 Here, we describe the discovery of two independent and extremely recent sex chromosome-
109 autosome fusions in one *D. virilis* strain, vir00. We hypothesize that this strain has been more
110 prone to DNA instability events, possibly caused by its excessive satellite DNA abundance. After
111 applying DNA replication and physical stressors, we measured DNA damage levels directly and
112 demonstrate that the DNA damage response is associated with satellite abundance. We use
113 two genetically identical strains that differ only by a chromosome fusion and satellite DNA
114 abundance, and demonstrate that the strain with more satellite DNA has significantly increased
115 DNA damage when stressed. Finally, we propose a model that genome instability may impose a
116 constraint on satellite abundance, a model that is entirely consistent with our data.
117
118 **RESULTS**
119
120 **Two novel sex chromosome Robertsonian translocations in *D. virilis* strain vir00**
121

122 In summer 2019, we performed DNA fluorescence in-situ hybridization (FISH) on larval
123 neuroblast nuclei of the vir00 strain that we had obtained several months earlier from the
124 National Drosophila Species Stock Center. We discovered it contained a Y-autosome fusion
125 (Figure 1A). The Y chromosome is recognizable in *D. virilis* because it has a distinct DAPI staining
126 intensity pattern, and contains a distinct arrangement of satellite DNA (Flynn *et al*. 2020).
127 However, all other chromosomes are difficult to distinguish in metaphase spreads, so we could
128 not immediately determine the fusion partner. We observed that the fused chromosome
129 contained the same centromere-proximal satellite as the Y chromosome, AAACTAT. To
130 determine if this chromosome fusion was present in other strains from similar geographical
131 locations, we imaged larvae from strains vir08, vir86, and vir48, which were collected from
132 different localities in California and Mexico (vir00 was collected from California). No larvae
133 screened in these other strains contained any chromosome fusions. We designate the vir00
134 substrain with the Y fusion as vir00-Yfus.
135
136 In Fall 2019, we obtained a second stock of vir00 from the National Drosophila Species Stock
137 Center. We set up single pair crosses and performed larval neuroblast squashes to karyotype
138 multiple male progeny of each cross. Surprisingly, we found that the Y-autosome fusion was not
139 present in any of the larvae karyotyped. However, 3/10 crosses karyotyped contained a
140 different fusion. This new fusion contained the brightly-dapi-staining AAATTAC satellite as the
141 centromere-proximal satellite, indicating that it is completely distinct from the Y fusion and
142 involved different chromosomes. We hypothesized that this new fusion involved the X
143 chromosome for several reasons; 1) based on centromere satellite identity, it had a 67%
144 probability (Flynn *et al.* 2020); 2) it was found only in single copy in male larvae, but sometimes
145 two copies in female larvae; 3) it was associated with observed X-Y nondisjunction events, such
146 as the presence of an XXYY female (Figure S1). We performed single-pair crosses and screened
147 the resulting progeny until we isolated a substrain fixed for the X fusion, and called this
148 substrain vir00-Xfus. We maintained one of the cross descendants from the 2019 stock that did
149 not have any evidence of the X fusion, which we designate vir00-Nofus. We inferred that both X
150 and Y fusions likely represent canonical Robertsonian translocations, in which two acrocentric

151 chromosomes that underwent DNA breakage were fused together at the centromere during
152 repair.

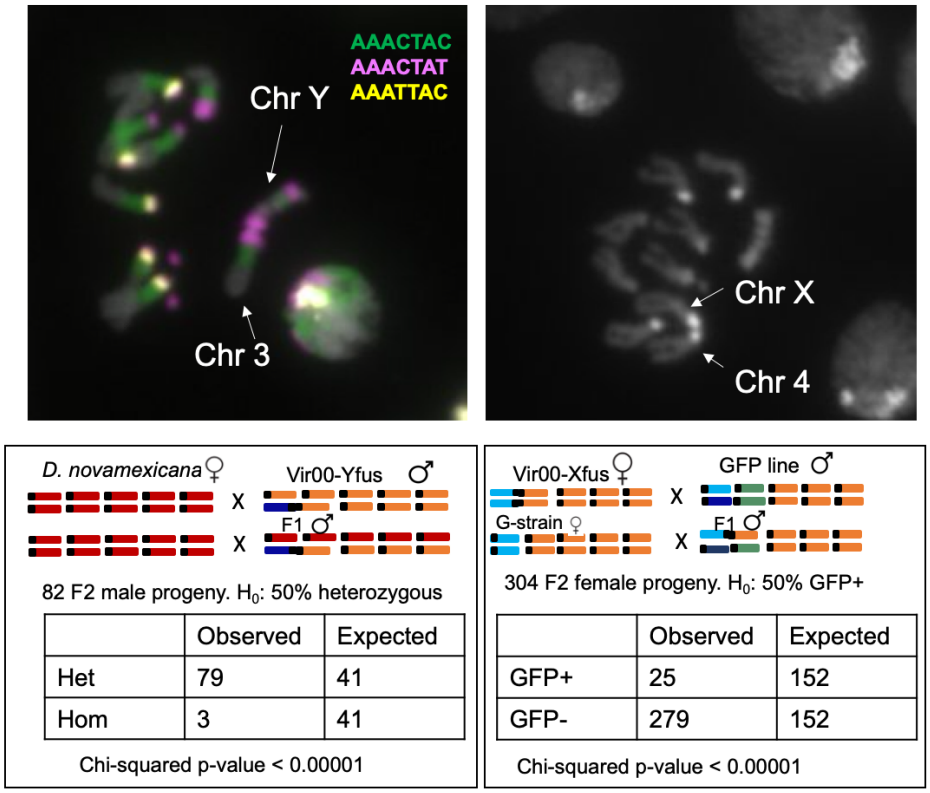

	Observed	Expected
Het	79	41
Hom	3	41

Chi-squared p-value < 0.00001

	Observed	Expected
GFP+	25	152
GFP-	279	152

Chi-squared p-value < 0.00001

153
154
155 **Figure 1**. Discovery and genetic validation of two independent fusion events in vir00. A) DNA-
156 FISH in metaphase chromosome squashes demonstrating the Y fusion. B) DAPI staining of
157 metaphase chromosome squashes demonstrating the X-4 fusion. C) Genetic validation of the Y-
158 3 fusion and D) the X-4 fusion. Red chromosomes: *D. novamexicana*; orange: wildtype *D. virilis*
159 autosomes; green: autosome containing a GFP marker; light blue: X chromosome; dark blue: Y
160 chromosome.
161
162 **Genetic validation revealed Y-3 and X-4 fusions**
163
164 We designed two separate two-generation crossing experiments to validate the fusions
165 genetically and identify the autosome each sex chromosome is fused to. Both experiments
166 exploited autosomal markers which we could determine if they were segregating non-
167 independently of sex. The first experiment to validate the Y-autosome fusion used crosses
168 between vir00-Yfus and *D. novamexicana* and scoring of microsatellite loci on each candidate
169 autosome. We scored 82 F2 male progeny for the Chr3 marker, and 79/82 contained both
170 alleles, whereas the null hypothesis was 50% should contain both alleles (Figure 1C, Figure S2).

171 The three progeny that did not contain both alleles were determined to have nondisjunction
172 events and did not contain the Y chromosome (Figure S3). We concluded that the Y
173 chromosome is fused to Chr3, and that the fusion was fixed in this subline. The other markers
174 on Chr2, Chr4, and Chr5 segregated independently of sex and acted as negative controls (Table
175 S1). We also did a negative control with the same crossing scheme except with vir08 instead of
176 vir00 (Chr3 chi-square p = 0.39, N=22, Table S1).
177
178 The second experiment to validate the X-autosome fusion used crosses to *D. virilis* transgenic
179 lines containing GFP markers on one of each of the candidate autosomes. For the crosses to
180 Chr4-GFP (vir95), we phenotyped 304 F2 female progeny, and found that progeny containing a
181 GFP signal were significantly depleted compared to the Mendelian expectation of 50% (Figure
182 1D). This indicated that the X chromosome was fused to Chr4. This crossing scheme with two
183 other candidate autosomes did not show association of GFP signal with sex (Chi-square p-value
184 > 0.1, Table S2). We also performed a negative control with the *D. virilis* genome strain instead
185 of vir00-Xfus crossed to the Chr4-GFP line and found the GFP signal was independent of sex
186 (Chi-square p-value = 0.92, Table S2).
187
188 We validated that vir00-Yfus and vir00-Xfus are the same genetic line and not the result of
189 contamination from other lines either in our lab or the stock center. We made use of medium-
190 coverage whole genome sequencing from Flynn et al. (2020) to design primers to amplify
191 singleton insertion/deletion variants present only in vir00 (the version that was sequenced was,
192 in hindsight, vir00-Yfus) and not in any other wildtype *D. virilis* strain present in the stock center
193 (Table S3). We designed primers to amplify four loci on chromosomes 2, 3, 5, and 6 which
194 contain a homozygous 12-13 bp deletion in vir00 compared to the reference and the other
195 strains (Table S4). We found that both versions of vir00 contained the deletion at each of these
196 loci, confirming that these substrains are indeed the same strain and not a contamination
197 (Figure S4). Although we did the above indel experiment first, the whole genome resequencing
198 SNP analysis (below) was also concordant with these substrains being the same genetic line.
199

200 **Satellite DNA decreased in vir00-Nofus compared to vir00-Yfus**

201

202 We used Illumina to resequence the three vir00 substrains: vir00-Yfus, vir00-Xfus, and vir00-
203 Nofus. We then used k-Seek to quantify the satellite abundance in each substrain (Wei *et al.*
204 2014). Assuming the most ancestral strain was vir00-Yfus, we found that satellite abundances
205 decreased in the two derived lines vir00-Xfus and vir00-Nofus (Table S5). In vir00-Xfus, there
206 was an 8% decrease only in the centromere proximal satellite of ChrX and Chr4 (AAATTAC).
207 vir00-Nofus had an overall 12% loss of satellite DNA compared to vir00-Yfus (Figure 3b). vir00-
208 Nofus had a similar 8% decrease in AAATTAC, in addition to a 10% loss in the pericentromeric
209 satellite (AAACTAC) and a 13% loss in the centromere-proximal satellite of ChrY and Chr3
210 (AAACTAT). These data are consistent with our interpretation that vir00-Nofus is the result of
211 breaking apart of the fusion chromosomes, and we conclude that significant satellite DNA was
212 lost from all three pericentromeric and centromeric satellites in vir00-Nofus.

213

214 **DNA damage levels in response to stress is related to satellite abundance in *D. virilis***

215

216 The vir00 strain, with the highest abundance of satellite DNA, contained two recent
217 independent Robertsonian translocations. There are multiple steps required to detect a
218 Robertsonian translocation: DNA breakage near the centromere, repair and fusion with another
219 acrocentric chromosome, retention of a functional centromere, and intergenerational
220 retention. To isolate the first step and the fundamental process in genome instability, we
221 sought to measure DNA breakage directly. Since vir00-Yfus also contained the highest
222 abundance of satellite DNA compared to the other strains, we wanted to test if variation in DNA
223 breakage level after stress was associated with satellite DNA abundance. We therefore
224 measured DNA damage levels in 7 different *D. virilis* strains, including vir00-Yfus and vir00-
225 Nofus, with varying abundances of satellite DNA in response to replication stress and low-level
226 radiation.

227

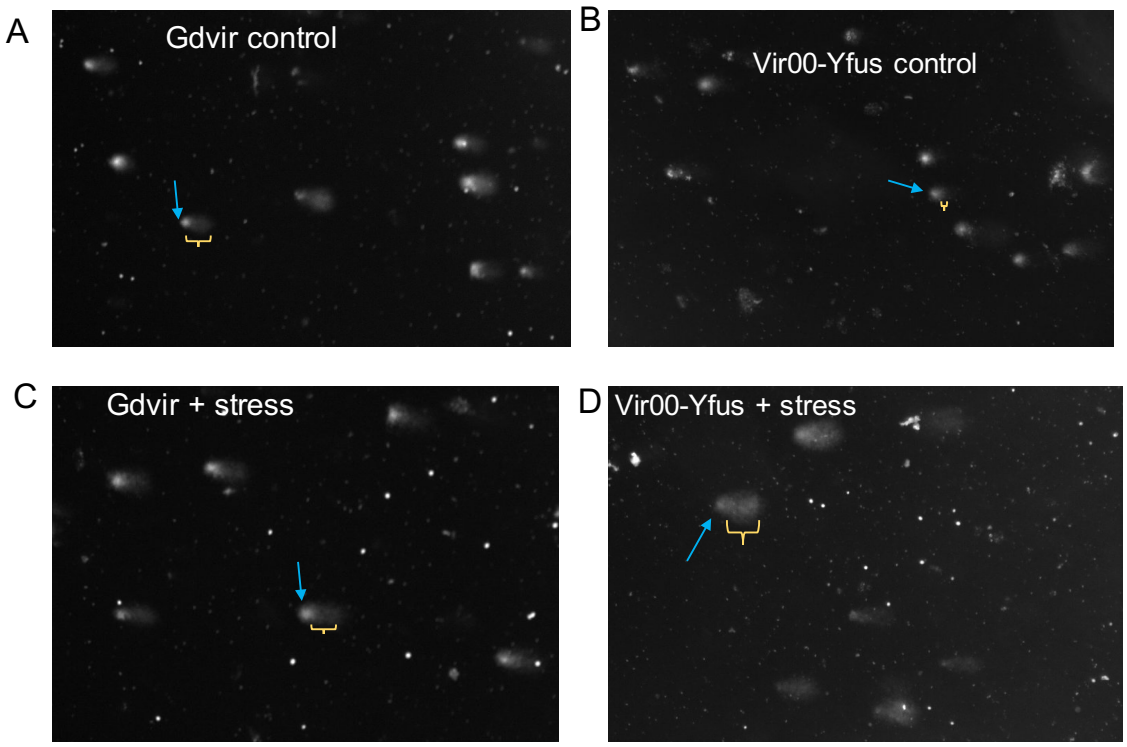

Figure 2. Comet assay images of nuclei isolated from *D. virilis* adult testes of the genome strain vir87 (A/C) and from vir00-Yfus (B/D) with and without stress (gemcitabine + radiation). Blue arrows point to the comet head and yellow brackets indicate the comet tails. The comet head and tail distribution for GDvir are of similar size and intensity. In vir00-Yfus, the comet tail is largely diffuse and expanded in the stress conditions compared to the control. These strains represent the lowest and highest satellite DNA abundances which have the least and greatest increase in DNA damage in response to stress, respectively.

Since spontaneous DNA breakage events are rare and we did not want to confound our data with breaks that occur as part of meiotic crossing over, we used stressors to elevate the rate of DNA damage. This would allow us to potentially detect a difference in the phenotype of interest between strains and also amplify possible types of stress imposed by excess satellite DNA content. We fed 0-1 day old adult flies the nucleoside analog gemcitabine for 8 days, which stalls replication forks and acts as a sensitizer for radiation via the Rad51 pathway (Kobashigawa *et al.* 2015). We then irradiated these sensitized flies with gamma rays at low level radiation (10 Gy). For each of seven strains tested, we included a control which was fed with the same liquid food with no gemcitabine and did not receive radiation treatment. We used the comet assay or single-cell gel electrophoresis to measure DNA damage in the male

248 germline in each line (Figure 2). We quantified comets using OpenComet software and used the
249 olive moment measurement as the statistic representing DNA damage (Gyori *et al.* 2014) (Table
250 S6). To detect differences in DNA damage in response to stress between strains, we took the
251 mean difference in olive moments between the control and stress treatments (see Methods).
252
253 The strain with the lowest satellite abundance, the genome strain, contained the lowest DNA
254 damage response and this was significantly lower than all other strains tested (Figure 2A,C,
255 Figure 3A). The strain with the highest satellite abundance, vir00-Yfus, had among the highest
256 DNA damage responses (Figure 2B,D), but was not significantly different from two other strains
257 vir8 and vir48 (Figure 3A). Like most other phenotypes, there are likely multiple genetic factors
258 contributing to the variation we found. Ideally, to demonstrate that satellite DNA is a causal
259 factor, we would manipulate satellite DNA abundance and test the DNA damage phenotypes,
260 but multi-megabase long arrays of satellite DNA cannot be manipulated with traditional
261 genome editing. However, vir00-Yfus and vir00-Nofus differ only by a chromosome fusion and
262 12% satellite abundance. Thus, if there is a difference in DNA damage response between these
263 substrains, it may be caused by differing satellite abundance. vir00-Nofus, which contained 12%
264 less satellite DNA than vir00-Yfus, had a significantly reduced DNA damage response, which is
265 concordant with our expectations that satellite DNA plays a causal role (Figure 3B).
266

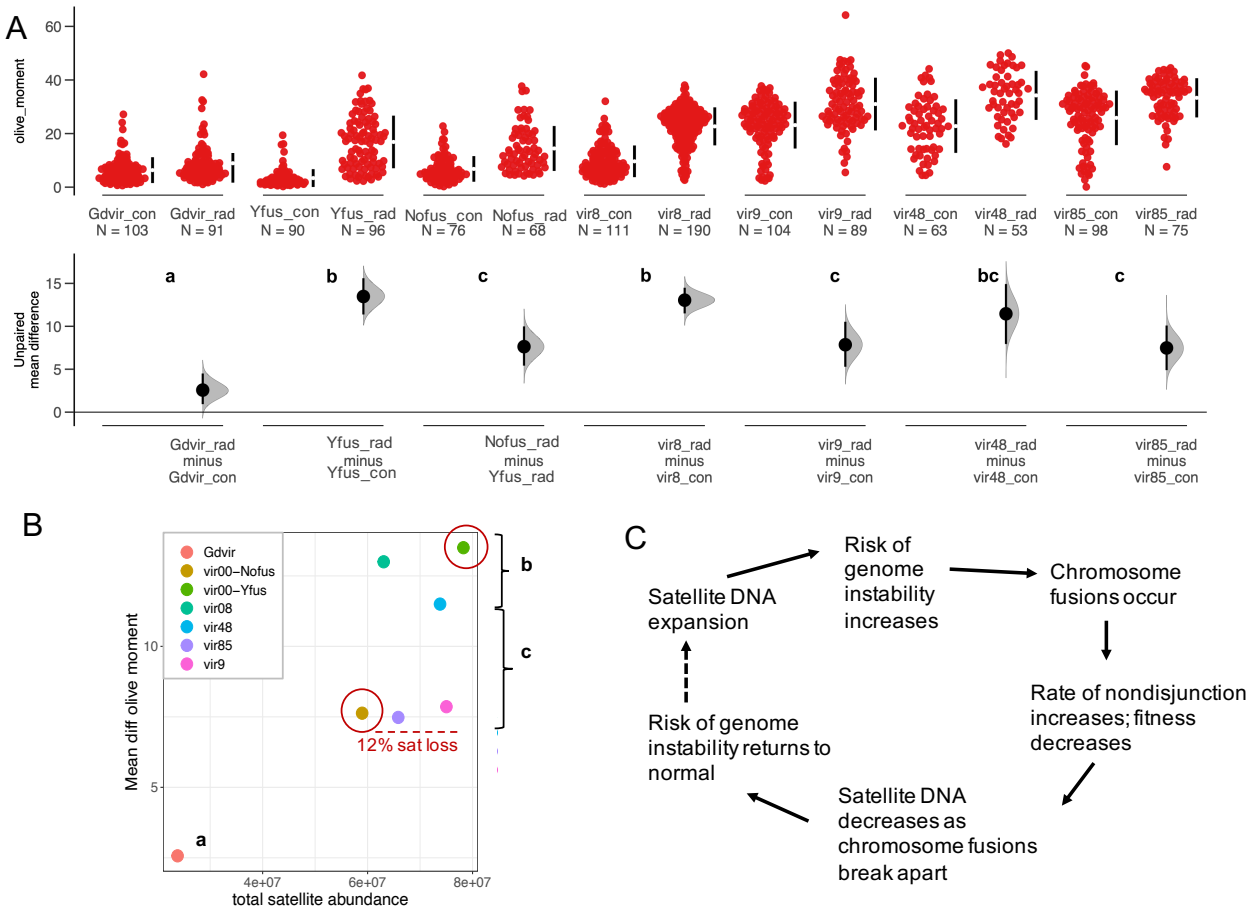

Figure 3. Satellite DNA is associated with DNA breakage in response to stress. A) Olive moment, a statistic of the comet assay, measuring DNA damage for 7 different strains paired with a control and stress treatment. N indicates the number of nuclei analyzed for each treatment. Flies treated with gemcitabine and radiation are suffixed with "rad" and control flies are suffixed with "con". The lower panel shows the unpaired mean difference between "rad" and "con" for each fly strain (black dot) and 95% confidence intervals (black line) produced from dabestr (5000 bootstrap method). Groups a, b, and c indicate samples with overlapping confidence intervals. B) The satellite DNA abundance of each *D. virilis* strain (x axis) and its unpaired mean difference between treatment and control (y axis). vir00-Nofus experienced a 12% loss in satellite DNA compared to vir00-Yfus, which is associated with a significantly decreased DNA damage in response to stress. C) Model that is consistent with our observations and data.

Extremely minimal degradation of the neo-Y chromosome

The Y-fused version of Chr3 is expected to accumulate mutations independently of the autosomal version of Chr3 over time because of the halt in recombination in male flies. This

287 would be represented in the mapping of short-read sequencing data by elevated heterozygosity
288 on Chr3. Specifically, if the mutations arose after the fusion of Chr3 to the Y, they would not be
289 present in any other strains of virilis, assuming no recurrent mutation. Thus, we used GATK
290 genotyping and found heterozygous singletons unique to vir00-Yfus compared to other non-
291 vir00 strains on each autosome (Table S3). We found that the number of heterozygous
292 singletons was modestly but significantly enriched on Chr3 in vir00-Yfus: 2.45 SNPs/Mb more
293 than other autosomes (permutation test, $p < 0.001$). We suggest this elevated density of
294 singleton heterozygous sites may be due to the fusion with the Y chromosome and lack of
295 recombination over several generations. Assuming the enrichment was caused only by the Y-
296 fusion and that the neo-Y (Chr3) evolved clonally in a single lineage, we roughly estimate the Y-
297 3 fusion occurred 1000-2000 generations ago.
298
299 Because the X-4 fusion was segregating with the no-fusion karyotype, recombination in
300 heterozygotes would prevent degeneration of the neo-Y version of Chr4. Furthermore, we
301 believe the X-4 fusion occurred between 2018-2019 since it was not present in the stock we
302 obtained in 2018. We did not observe an enrichment of heterozygous singletons on Chr4 in
303 vir00-Xfus. However, there was still a slight enrichment on Chr3 in vir00-Xfus (1.45 SNPs/Mb,
304 permutation test $p = 0.031$), supporting our assumption that vir00-Xfus is the result of the
305 breaking apart of the Y fusion and forming a new fusion.
306
307 **Nondisjunction between the X and Y chromosomes is highly elevated in chromosome fusion**
308 **lines**
309
310 Nondisjunction occurs when homologous chromosomes fail to separate at meiosis, and results
311 in aneuploidy in the progeny. Autosomal and X chromosome aneuploidy is lethal in flies; but Y
312 chromosome aneuploidy is viable: females that have a Y chromosome (XXY) are fertile, males
313 with no Y chromosome (XO) are sterile, and males with two Y chromosomes (XYY) are fertile.
314 Elevated rates of X-Y nondisjunction represent a fitness cost because zygotes with infertile or
315 lethal karyotypes will form at increased frequency. We found some evidence of nondisjunction

316 in the vir00-Yfus genetic validation (Figure S3), and also common Y chromosome aneuploidy in
317 the stock of vir00-Xfus (Figure S1). Since both fusions involve the sex chromosomes, we tested
318 the rate of primary X-Y nondisjunction in males in all three versions of vir00, along with the *D.*
319 *virilis* genome strain as a control. We first fully isolated the vir00-Nofus strain to ensure no
320 fusion chromosomes were segregating, which even at low frequency could increase the rate of
321 nondisjunction in the line.
322
323 We crossed individual males of each strain to genome strain females and genotyped for the
324 presence or absence of the Y chromosome in progeny. Female progeny containing a Y
325 chromosome indicate XY sperm from the father, and male progeny lacking a Y chromosome
326 indicate nullisomic sperm from the father. Since nondisjunction was extremely high in vir00-
327 Xfus, 2/7 fathers tested were of XYY karyotype, which we could infer if more than half of his
328 female progeny contained a Y chromosome (Maggert 2014). We eliminated these fathers'
329 progeny from the primary nondisjunction rate calculation. No fathers tested from other
330 sublines were determined to be XYY. Males without a Y chromosome would not produce
331 progeny. We found that vir00-Yfus had a slightly elevated nondisjunction rate of 4.5%,
332 compared to the genome strain control of 1.2%, but it was not statistically significant with the
333 sample sizes we used (Table 1). vir00-Xfus had an extremely high primary nondisjunction rate of
334 21% (e.g. Figure S5), which was significantly higher than that of all other substrains ($p < 0.004$,
335 pairwise proportion test, Table 1). Surprisingly, vir00-Nofus had a significantly elevated
336 nondisjunction rate compared to the genome strain control, at 5.7%. This was not statistically
337 different from vir00-Yfus.
338

339
340 **Table 1**: Nondisjunction of the X and Y chromosomes in males is elevated in chromosome
341 fusion lines.
342
343

Line	Nondisjunction rate	Fathers with nondisjunction/ total fathers	Aneuploid progeny/ total progeny	Significance group
GDvir	1.2%	1 / 10	3 / 248	a
vir00-Yfus	4.5%	4 / 7	9 / 198	ab
vir00-Nofus	5.7%	4 / 6	11 / 192	b
vir00-Xfus*	21%	5 / 5	27 / 127	c

344
345
346 *only including primary nondisjunction
347
348
349 **Discussion**
350
351 *D. virilis* has the highest relative satellite DNA abundance of any studied species. Is there a
352 maximum limit of satellite DNA a genome can tolerate before there are negative
353 consequences? We found that vir00, the strain with 15% more pericentromeric satellite DNA
354 than other strains recently underwent two independent chromosome fusion events. vir00-Yfus
355 has the highest satellite DNA abundance and among the highest DNA damage level in response
356 to stress. vir00-Nofus, with 12% less satellite DNA, which was presumably lost in the breaking
357 apart of the chromosome fusions, has significantly lower DNA damage level in response to
358 stress. We propose a model that places a constraint on satellite DNA abundance and can
359 explain our findings with the vir00-line (Figure 3C). If satellite DNA expands, the risk of DNA
360 breakage and genome instability increases and chromosome fusions may occur. These
361 chromosome fusions may increase the nondisjunction rate and make the affected line less fit.
362 The chromosome fusions may later break apart; and as this occurs pericentromeric satellite
363 DNA may be lost (Figure 3C). This in turn results in a decreased risk of genome instability. The

364 question of whether satellite DNA abundance influences genome instability has had
365 considerable interest recently (Arora *et al.* 2021), however a convenient system in which to test
366 this question has been lacking.
367
368 There are several possible mechanisms that might cause excess satellite DNA to increase the
369 risk of DNA breakage. Satellite DNA may form complex structures, loops, or non-B DNA, and
370 increasing the length of the arrays may make these regions more unstable in cis (Barra and
371 Fachinetti 2018). It may be challenging for polymerases to replicate many megabases of
372 tandem satellite sequence, and longer arrays may have a higher risk of stalling polymerases and
373 thus DNA breaks in cis (Barra and Fachinetti 2018). Finally, increased satellite DNA may titrate
374 away binding proteins that maintain genome stability, in trans (Francisco and Lemos 2014;
375 Brown *et al.* 2020a; Giunta *et al.* 2021). Whether there is a maximum threshold of satellite
376 array length or abundance, as suggested in Charlesworth *et al.* (1986), or whether risk of
377 genome instability varies continuously with satellite abundance will require further study.
378
379 Chromosome rearrangements such as Robertsonian translocations are rare occurrences, but
380 are commonly the cause of karyotype evolution between species (Mayrose and Lysak 2021). In
381 humans, rearrangements resulting from breaks near the centromere are associated with
382 miscarriages and in the case of somatic rearrangements, cancer (Barra and Fachinetti 2018).
383 Previous studies have found repetitive element involvement in chromosome rearrangements in
384 multiple species (Paço *et al.* 2015; Reis *et al.* 2018). However, genetic variation of repetitive
385 DNA within species has never been associated with increased risk of genome instability. Here
386 our data suggests, at least in *D. virilis* strain vir00, that elevated satellite DNA may play a causal
387 role in increasing the risk of DNA breakage, which can lead to deleterious rearrangements.
388
389 We identified elevated nondisjunction rates as a cost of chromosome fusions. Surprisingly, the
390 rate of nondisjunction was 5-fold higher in vir00-Xfus compared to vir00-Yfus. With a
391 nondisjunction rate of 21%, a significant proportion of abnormal karyotypes will be produced,
392 such as XO (sterile), XYY (viable and fertile), and XXY or XXYY (viable and fertile), all of which we

393 found in cytological samples. Further mating between these abnormal karyotypes will produce
394 significant proportions of sterile or inviable karyotypes like XYYY or XXX, which will further
395 decrease the fitness of this line. Furthermore, karyotypes with extra Y chromosomes such as
396 XYY and XXY have been found to have decreased lifespan (Brown *et al.* 2020b). Although we did
397 not assay the nondisjunction rate of the fused autosome, it is possible the nondisjunction rate
398 of Chr4 is also elevated in vir00-Xfus, which would further decrease the fitness of the line
399 because Chr4 aneuploidy is expected to be lethal (Lindsley *et al.* 1972). The extreme
400 nondisjunction rate indicates X-Y pairing is severely disrupted due to the X-4 fusion, but only
401 slightly if at all due to the Y-3 fusion. When the Y fusion presumably broke apart and the X
402 fusion formed, it is possible other rearrangements on the X and/or Y occurred that disrupted
403 pairing. Furthermore, the nondisjunction rate did not decrease to a level similar to the genome
404 strain in vir00-Nofus. We believe this indicates a remaining rearrangement in vir00-Nofus
405 affecting the pairing and disjunction of the X-Y. We only found a modest difference in estimated
406 rDNA copy number between the substrains (Table S7), which has been found to mediate pairing
407 of the X and Y (McKee and Karpen 1990). Detailed analysis of structural rearrangements in the
408 heterochromatin will be required to determine the mechanism of the elevated nondisjunction
409 rates.
410
411 Our study has several limitations. First, the vir00-Nofus flies we used for resequencing and for
412 DNA damage assays had the X-4 fusion segregating at low frequency (<15%), which was
413 unknown to us until we were able to correct it for the nondisjunction assays. However, we
414 believe our results hold firmly because the main comparison was with vir00-Yfus, the substrain
415 with the most satellite DNA. For testing our hypothesis, the fusion status in the other substrains
416 matters less than the satellite DNA abundance, which was markedly lower in the vir00-Nofus
417 substrain we used. Furthermore, the increase in damage level between the control and stressed
418 flies may not be directly applicable to the risk of DNA breaks and genome instability in natural
419 conditions. Although we find a difference in the DNA damage in response to stress between
420 vir00 substrains with different abundances of satellite DNA, their fusion status is also different.
421 We cannot eliminate the possibility that the presence of the Y fusion itself increased the rate of

422 DNA damage instead of the abundance of satellite DNA. Finally, we cannot eliminate the
423 possibility that satellite DNA increased in vir00-Yfus after the fusion occurred and not prior to as
424 we suggest in our model.
425
426 We believe the system we discovered will be useful for a variety of future studies. The vir00
427 fusion substrains will be useful for studying centromere identity. In both the Y-3 and X-4
428 fusions, two spherical regions of satellite DNA are present at the centromere of these fusions,
429 representing one from each acrocentric chromosome (Figure 1). We note that the X-4 fusion in
430 vir00 is homologous to an independent X-4 fusion in *D. americana* 29 thousand years ago, a
431 species only 4.5 million years diverged. In the X-4 fusion of *D. americana*, there is only one
432 discrete region of centromeric satellite (Flynn *et al.* 2020), unlike what we found here. In female
433 meiosis where chromosomes can compete to get into the oocyte rather than the polar body,
434 "stronger" centromeres with more satellite may have an advantage. A "supercentromere"
435 resulting from a centromere-centromere fusion is one way to do this, and in *D. americana* the
436 X-4 fusion has biased transmission into the egg (Stewart *et al.* 2019). Finally, since both
437 centromere-centromere fusions had matching centromere-proximal satellites (AAACTAT for Y-3
438 and AAATTAC for X-4), we suggest that the centromeric satellite identity is important for DNA
439 repair for Robertsonian translocations, or for stability and retention of the centromere.
440
441 **METHODS**
442
443 Scripts required to reproduce the computational results are available here:
444 https://github.com/jmf422/D-virilis-fusion-chromosomes
445
446 **Neuroblast squashes and satellite DNA FISH**
447
448 We dissected brains from wandering 3rd-instar larvae and performed the fixation steps as in
449 (Larracuente and Ferree 2015). Specifically, we placed brains in sodium citrate solution for 6
450 minutes before fixation. After fixation and drying of slides, we applied Vectashield dapi

451 mounting medium. We performed DNA-FISH on vir00-Yfus, which allowed us to confidently
452 identify the Y chromosome based on its unique satellite DNA composition. We used the same
453 fixation and staining protocol as Flynn *et al.* (2020). We imaged metaphase cells using a 100x oil
454 objective on an Olympus fluorescent microscope and Metamorph capture system at the Cornell
455 Imaging Facility.
456
457 **Y-autosome fusion validation**
458
459 We designed an experiment that would both validate the Y chromosome fusion and to
460 distinguish which autosome is fused. We first designed primers flanking microsatellite loci on all
461 four autosomes that met the following criteria: 1) had 100% conserved non-repetitive and
462 unique priming sites between *D. virilis* and *D. novamexicana*; 2) amplicon length differed
463 between the species by at least 15 bp as to be distinguished on an agarose gel; 3) locus
464 contained a mono or tri nucleotide repeat; 4) locus length ~200 bp. We next set up a two-
465 generation crossing scheme (Figure 1A). We crossed *D. novamexicana* virgin females with vir00-
466 Yfus males and selected the male progeny, which we backcrossed to *D. novamexicana* virgin
467 females. We then genotyped the male F2 progeny from this cross at the 4 sets of primers
468 corresponding to the four non-dot autosomes (Chr2, 3, 4, 5) (Table S4). We performed single-fly
469 DNA extraction in strip tubes with Tris-EDTA buffer and 0.2 mg/mL proteinase K. We did 12 uL
470 standard PCR reactions (3 min at 95, 30 cycles of 30 sec 95, 30 sec 55, 50 sec 72, final extension
471 5 min). Each primer on each PCR plate had a homozygous (*D. novamexicana*) and heterozygous
472 (*D. novamexicana-D.virilis* F1 hydrid) control. We then ran the PCR product on 2.5% agarose
473 gels. If there was indeed an autosome fused to the Y chromosome, we would expect to see
474 100% of the male progeny being heterozygous for the *virilis* and *novamexicana* alleles (except
475 for rare cases of non-disjunction). For the autosomes that are not fused, we would expect to
476 see 50% of the progeny being homozygous for the *novamexicana* allele, and half heterozygous,
477 due to Mendel's law of random segregation. We successfully validated the existence of the Y
478 fusion, and found that it is fused to chromosome 3 (Muller D) (Table S1, Figure 1). There were 3
479 male progeny that were homozygous for the Chr3 *novamexicana* allele. We verified that these

480 were cases of nondisjunction (opposed to the Y fusion not being fixed in this subline) by finding
481 that the Y chromosome was absent in controlled Y chromosome PCR assays (Figure S3).
482
483 **Isolation of vir00-Xfus and vir00-Nofus**
484
485 The X fusion was found to be segregating with a no fusion substrain in the 2019 stock of vir00.
486 We wanted to isolate these into two separate substrains where the karyotype is fixed. From the
487 progeny of the three original crosses in which we found the X fusion, we made 10 single pair
488 crosses and did neuroblast squashes of 6-8 larval progeny per cross, including both sexes. By
489 chance, we should be able to find a cross in which the mother had two copies of the fusion and
490 the father had a single copy – in which the derived line would be fixed for the fusion. If all
491 progeny imaged contained the fusion (and females contained two copies of the fusion), then it
492 is likely that this was the case. We created this line, and call it vir00-Xfus. We maintained a line
493 isolated from the 2019 stock that had no evidence of the X fusion and called it vir00-Nofus. We
494 later found that vir00-Nofus still had the X fusion segregating at low frequency. We isolated a
495 fixed Nofus version in the same way as above for nondisjunction assays, because a low
496 frequency fusion could increase the nondisjunction rate greatly.
497
498 **X-autosome fusion validation**
499
500 We obtained transgenic strains with GFP (or Blue) insertions which are expressed in the eye and
501 larval brain from the National Drosophila Species Stock Center (vir95, vir121, vir117). Stern *et*
502 *al.* (2017) found the insertion sites of these lines. We chose lines which contained the GFP
503 marker on candidate autosomes Chr2, Chr4, and Chr5. Chr3 was not a candidate because it is
504 fused to the Y in vir00-Yfus and contains a different centromeric satellite. Before setting up
505 crosses, we screened 10-20 larvae of each line with a fluorescent microscope to ensure the
506 transgene had not drifted to low frequency. Larvae containing the transgene demonstrated the
507 GFP signal in their brain. We chose to phenotype at the larval stage since we would be crossing
508 GFP strains to wildtype red-eyed flies and the visibility of GFP in the adult eye would be low. We

509 then designed a crossing scheme which would allow us to both validate that the X chromosome
510 was fused and distinguish which autosome it was fused to (Figure 1B). We crossed GFP-line
511 males to vir00-Xfus virgin females. We then selected the male F1 progeny and crossed them to
512 virilis genome strain virgin females. We then phenotyped F2 larvae, classifying each as either
513 GFP positive or negative. When the phenotyped flies emerged, we sexed and counted them. If
514 the candidate autosome is fused to the X, we would expect sex to segregate with the GFP
515 marker: all female progeny will be GFP negative, and all male progeny will be GFP positive
516 (except for phenotyping errors or rare nondisjunction events). For all other lines, sex should not
517 segregate with GFP status. We performed negative control crosses in which the parental cross
518 was replaced by genome strain virgin females, to ensure the crossing scheme produced the
519 expected results (Table S2). We found that the X chromosome is fused to Chr4 (Muller B).
520
521 **Validation of the three versions of vir00 with private fixed indels**
522
523 We used GATK recommended practices to do genotyping of our low-coverage whole genome
524 sequencing data from Flynn et al. (2020). We used vcftools to subset singletons present only in
525 vir00, which was, in hindsight, vir00-Yfus. We then used GATK's SelectVariants to select only
526 non-reference homozygous indels 12 bp or more with a depth of at least 10 in vir00 and at least
527 2 in the other strains. We then manually inspected each potential candidate in IGV to ensure:
528 no reads in other strains supported the indel, all reads in vir00 supported the indel, and there
529 were no nearby indels in other strains. We then designed primers for the four loci (on Chr 2, 3,
530 5, 6) that met these criteria and also had enough SNP-free sequence flanking the indel in order
531 to design primers that would amplify a locus 100-200 bp equally in all strains. We performed
532 PCR and gel electrophoresis (2.5% gel, 98 V, 90 min).
533
534 **DNA damage assays**
535
536 We chose two stressors that would moderately increase the rate of DNA breaks and allow us to
537 potentially detect differences between strains. Gemcitabine is a nucleoside analog that induces

538 replication stress by stalling polymerases, and also sensitizes cells to radiation via the RAD51
539 pathway (Kobashigawa *et al.* 2015). We selected dosage and a fly-feeding regime based on
540 (Kislukhin *et al.* 2012). Ionizing radiation has long been used to increase the rates of DNA breaks
541 in flies for mutagenesis. We chose a dose ¼ - ½ of what has been typically used in mutagenesis
542 (Carlson and Southin 1962).
543
544 We collected male flies 0-1 days old and fed them gemcitabine (0.718 mM) mixed with liquid
545 food in vials with 8-12 adult flies as in (Kislukhin *et al.* 2012). Liquid food consisted of 12.5g
546 sucrose, 17.5 g dry yeast, 5 mL corn syrup, and 95 mL PBS (autoclaved for 30 min immediately
547 after adding the yeast). Flies were fed the drug for 7-9 days before radiation. Controls were fed
548 with the same liquid food for 7-9 days, except no gemcitabine was added. Flies were moved to
549 fresh vials every 3-4 days. For radiation treatment, we transferred flies into 50 mL conical tubes
550 with 5 mL agar because these tubes were compatible with the radiation source. Control flies
551 were also transferred to new tubes. We used a J.L. Shepherd & Associates Mark I Irradiator with
552 1,100 Ci of Cs-137, and flies were irradiated at approximately 400 rad/min for a total of 10 Gy.
553 In one case, for the GDvir stress treatment, the radiation was not stopped on time so 4 extra Gy
554 were applied. We believe this did not affect our results, especially because the GDvir strain had
555 the lowest DNA damage increase with gemcitabine and radiation stress. We did comet assays
556 to measure DNA damage (Angelis *et al.* 1999) over three different dates (Table S6), but ensured
557 experimental conditions were practically identical each time. For some samples we had to
558 combine results from two different dates to have enough nuclei for statistical analysis (Table
559 S6). We dissected testes from approximately 8 flies from each treatment within one hour of
560 radiation treatment to minimize the opportunity for breakage repair (Shetty *et al.* 2017). We
561 then homogenized the testes tissue using a dounce, filtered the homogenate through a 40
562 micron filter to remove debris, and centrifuged and resuspended the cells to approximately 10^5
563 cells/mL.
564
565 We next performed the alkaline comet assay as directed by the Enzo comet kit (ADI-900-166),
566 which provides higher sensitivity than the neutral comet assay (Angelis *et al.* 1999). We imaged

567 slides on a metamorph imaging system at 10x magnification using a fluorescent green filter to
568 detect the CyGreen dye included in the comet kit. We quantified damage levels using the
569 software OpenComet as a plugin in ImageJ (Gyori *et al.* 2014). We filtered called nuclei that
570 were not comet shapes or contained background interference. We used the measure of "olive
571 moment," which is the product of the percent of DNA in the tail and distance between
572 intensity-weighted centroids of head and tail (Gyori *et al.* 2014) as the statistic to compare
573 between strains and treatments.
574
575 **Resequencing sublines to determine differences in their satellite abundance.**
576
577 Pools of 6 male flies were DNA extracted with Qiagen DNeasy blood and tissue kit. PCR-free
578 libraries were then prepared with Illumina TruSeq PCR-free library prep. Libraries were
579 sequenced on a NextSeq 500 single end 150 bp. We removed adapters and poly-G signal with
580 fastp and then ran k-Seek to count satellite abundances (Wei *et al.* 2014). We used average
581 read depth to normalize the kmer counts. We also mapped the reads to the *D. virilis* rDNA
582 consensus sequence (http://blogs.rochester.edu/EickbushLab/?page_id=602) to estimate the
583 rDNA copy number in the three vir00 substrains as well as a vir08 as a control (Table S3, S7).
584
585 **Using sequencing data to estimate the age of the Y-3 fusion**
586
587 Scripts for this section are available here: https://github.com/jmf422/D-virilis-fusion-
588 chromosomes/tree/main/simulate_degradation. We used the sequencing data from Flynn et al.
589 (2020) in addition to data produced here for vir00-Yfus, vir00-Xfus, and vir00-Nofus and 10
590 other *D. virilis* strains. We mapped the data to the RS2 genome assembly using bowtie2. We
591 then genotyped with GATK following standard procedures (McKenna *et al.* 2010). We extracted
592 heterozygous singleton sites for vir00, and counted how many occurred on each autosome. We
593 calculated the enrichment on Chr3 in vir00-Yfus based on the difference from the average SNP
594 density on the other autosomes (excluding the dot chromosome Chr6). To determine whether
595 this enrichment of SNPs was significant based on the size of the chromosome and the number

596 of mutations, we randomly permuted the total number of heterozygous singleton SNPs on all
597 autosomes and calculated the proportion falling on Chr3, and repeated this 1000 times.
598
599 We then performed simple simulations to determine approximately how many generations of
600 mutation accumulation without recombination or selection would result in the enrichment we
601 observed. Since heterozygous singletons are challenging for the genotyper to call with
602 moderate coverage sequencing data, we incorporated this into our simulation. First, we made
603 the genome assembly diploid then used mutation-simulator (Kühl *et al.* 2020) to simulate
604 random mutations (transition/transversion ratio 2.0) at a rate of 2×10^{-9} per bp per generation
605 for 500, 1000, 2000, and 5000 generations on one copy of Chr3 only. We then simulated
606 Illumina reads with ART (Huang *et al.* 2012) at the same depth as we have for vir00-Yfus in our
607 real data (23 x haploid or 11.5 x diploid). We next used standard GATK genotyping and selected
608 out heterozygous singletons on Chr3. We repeated the simulation 10 times for each number of
609 generations to get a range of values. The empirical enrichment fell in between what we found
610 in the simulations for 1000 and 2000 generations.
611
612 **Nondisjunction assays**
613
614 We crossed a single male from vir00-Yfus, vir00-Xfus, vir00-Nofus (fixed), and GDvir (control) to
615 one or two GDvir (genome strain vir87) females. We collected the virgin progeny from each
616 cross, extracted DNA with a squish-proteinase K prep, and genotyped with PCR and gel
617 electrophoresis for the presence or absence of the Y chromosome in up to 16 female and 16
618 male progeny. We amplified a locus unique to the Y chromosome (primers designed by Yasir
619 Ahmed-Braimah for a different project, Table S4). For a subset of individuals, we also
620 performed multiplex controls with an autosomal locus. Otherwise, we performed DNA
621 extractions in large batches with the same proteinase K mixture to minimize the chance of DNA
622 extraction failure. A very small quantity of DNA is required for a standard PCR with robust
623 primers. To control for the completeness of the PCR mastermix, we included male samples in
624 the same batch as female samples. If a male lacked a Y chromosome, we inferred the father's

625 sperm was missing the Y chromosome (nullisomic), and if a female contained a Y chromosome,
626 we inferred the father's sperm contained both X and Y. We used R prop.test to evaluate
627 whether there were any differences between nondisjunction proportions for the different
628 strains. After finding this highly significant, we used pairwise.prop.test in R with Holm-
629 Bonferroni multiple test correction to determine which pairs of substrain nondisjunction rates
630 were significantly different from each other.
631

632 **Acknowledgements**

633 We thank Yasir Ahmed-Braimah for discussions and use of primers. We greatly appreciate the
634 use of the Cs-137 irradiator from the Robert Weiss lab and to Amanda Loehr for operating the
635 device. Asha Jain prepared sequencing libraries for this project, and Yassi Hafezi provided
636 advice on the nondisjunction assays. We also thank members of the Clark lab for discussions
637 and encouragement on this project.
638

639 **References**
640

641 Anderson S. N., M. C. Stitzer, A. B. Brohammer, P. Zhou, J. M. Noshay, *et al.*, 2019 Transposable
642 elements contribute to dynamic genome content in maize. Plant J. 100: 1052–1065.

643 Anderson N. W., C. E. Hjelmen, and H. Blackmon, 2020 The probability of fusions joining sex
644 chromosomes and autosomes. Biol. Lett. 16: 20200648.

645 Angelis K. J., M. Dusinská, and A. R. Collins, 1999 Single cell gel electrophoresis: detection of
646 DNA damage at different levels of sensitivity. Electrophoresis 20: 2133–2138.

647 Arora U. P., C. Charlebois, R. A. Lawal, and B. L. Dumont, 2021 Population and subspecies
648 diversity at mouse centromere satellites. BMC Genomics 22: 279.

649 Bachtrog D., 2013 Y-chromosome evolution: emerging insights into processes of Y-chromosome

650 degeneration. Nat. Rev. Genet. 14: 113–124.

651 Balzano E., F. Pelliccia, and S. Giunta, 2020 Genome (in)stability at tandem repeats. Semin. Cell
652 Dev. Biol. https://doi.org/10.1016/j.semcdb.2020.10.003

653 Barra V., and D. Fachinetti, 2018 The dark side of centromeres: types, causes and consequences
654 of structural abnormalities implicating centromeric DNA. Nat. Commun. 9: 4340.

655 Bilinski P., P. S. Albert, J. J. Berg, J. A. Birchler, M. N. Grote, *et al.*, 2018 Parallel altitudinal clines
656 reveal trends in adaptive evolution of genome size in Zea mays. PLoS Genet. 14: e1007162.

657 Black E. M., and S. Giunta, 2018 Repetitive Fragile Sites: Centromere Satellite DNA As a Source
658 of Genome Instability in Human Diseases. Genes 9. https://doi.org/10.3390/genes9120615

659 Braekeleer M. D., and T.-N. Dao, 1990 Cytogenetic studies in couples experiencing repeated
660 pregnancy losses. Hum. Reprod. 5: 519–528.

661 Brown E. J., A. H. Nguyen, and D. Bachtrog, 2020a The Drosophila Y Chromosome Affects
662 Heterochromatin Integrity Genome-Wide. Mol. Biol. Evol. 37: 2808–2824.

663 Brown E. J., A. H. Nguyen, and D. Bachtrog, 2020b The Y chromosome may contribute to sex-
664 specific ageing in Drosophila. Nat Ecol Evol 4: 853–862.

665 Carlson E. A., and J. L. Southin, 1962 Comparative mutagenesis of the dumpy locus in
666 Drosophila melanogaster. I. X-ray treatment of mature sperm--frequency and distribution.
667 Genetics 47: 321–336.

668 Cechova M., R. S. Harris, M. Tomaszkiewicz, B. Arbeithuber, F. Chiaromonte, *et al.*, 2019 High
669 satellite repeat turnover in great apes studied with short- and long-read technologies. Mol.
670 Biol. Evol. https://doi.org/10.1093/molbev/msz156

671 Charlesworth B., C. H. Langley, and W. Stephan, 1986 The evolution of restricted recombination
672 and the accumulation of repeated DNA sequences. Genetics 112: 947–962.

673 Charlesworth B., and D. Charlesworth, 2000 The degeneration of Y chromosomes. Philosophical
674 Transactions of the Royal Society of London. Series B: Biological Sciences 355: 1563–1572.

675 Featherstone C., and S. P. Jackson, 1999 DNA double-strand break repair. Curr. Biol. 9: R759–
676 R761.

677 Ferree P. M., and D. A. Barbash, 2009 Species-specific heterochromatin prevents mitotic
678 chromosome segregation to cause hybrid lethality in Drosophila. PLoS Biol. 7: e1000234.

679 Flynn J. M., I. Caldas, M. E. Cristescu, and A. G. Clark, 2017 Selection Constrains High Rates of
680 Tandem Repetitive DNA Mutation in Daphnia pulex. Genetics 207: 697–710.

681 Flynn J. M., M. Long, R. A. Wing, and A. G. Clark, 2020 Evolutionary Dynamics of Abundant 7-bp
682 Satellites in the Genome of Drosophila virilis. Mol. Biol. Evol. 37: 1362–1375.

683 Francisco F. O., and B. Lemos, 2014 How Do Y-Chromosomes Modulate Genome-Wide
684 Epigenetic States: Genome Folding, Chromatin Sinks, and Gene Expression. Journal of
685 Genomics 2: 94–103.

686 Fry K., and W. Salser, 1977 Nucleotide sequences of HS-alpha satellite DNA from kangaroo rat

687 Dipodomys ordii and characterization of similar sequences in other rodents. Cell 12: 1069–
688 1084.

689 Gall J., E. Cohen, and M. Polan, 1971 Repetitive DNA sequences in Drosophila. Chromosoma 33.
690 https://doi.org/10.1007/bf00284948

691 Gall J. G., and D. D. Atherton, 1974 Satellite DNA sequences in Drosophila virilis. J. Mol. Biol. 85:
692 633–664.

693 Giunta S., S. Hervé, R. R. White, T. Wilhelm, M. Dumont, *et al.*, 2021 CENP-A chromatin prevents
694 replication stress at centromeres to avoid structural aneuploidy. Proc. Natl. Acad. Sci. U. S.
695 A. 118. https://doi.org/10.1073/pnas.2015634118

696 Gyori B. M., G. Venkatachalam, P. S. Thiagarajan, D. Hsu, and M.-V. Clement, 2014 OpenComet:
697 an automated tool for comet assay image analysis. Redox Biol 2: 457–465.

698 Huang W., L. Li, J. R. Myers, and G. T. Marth, 2012 ART: a next-generation sequencing read
699 simulator. Bioinformatics 28: 593–594.

700 Jagannathan M., R. Cummings, and Y. M. Yamashita, 2018 A conserved function for
701 pericentromeric satellite DNA. Elife 7. https://doi.org/10.7554/eLife.34122

702 Jagannathan M., and Y. M. Yamashita, 2021 Defective satellite DNA clustering into
703 chromocenters underlies hybrid incompatibility in Drosophila. bioRxiv 2021.04.16.440167.

704 Kislukhin G., M. L. Murphy, M. Jafari, and A. D. Long, 2012 Chemotherapy-induced toxicity is
705 highly heritable in Drosophila melanogaster. Pharmacogenet. Genomics 22: 285–289.

706 Kobashigawa S., K. Morikawa, H. Mori, and G. Kashino, 2015 Gemcitabine Induces
707 Radiosensitization Through Inhibition of RAD51-dependent Repair for DNA Double-strand
708 Breaks. Anticancer Res. 35: 2731–2737.

709 Kühl M. A., B. Stich, and D. C. Ries, 2020 Mutation-Simulator: Fine-grained simulation of
710 random mutations in any genome. Bioinformatics.
711 https://doi.org/10.1093/bioinformatics/btaa716

712 Larracuente A. M., and P. M. Ferree, 2015 Simple method for fluorescence DNA in situ
713 hybridization to squashed chromosomes. J. Vis. Exp. 52288.

714 Lindsley D. L., L. Sandler, B. S. Baker, A. T. Carpenter, R. E. Denell, *et al.*, 1972 Segmental
715 aneuploidy and the genetic gross structure of the Drosophila genome. Genetics 71: 157–
716 184.

717 Maggert K. A., 2014 Reduced rDNA Copy Number Does Not Affect "Competitive" Chromosome
718 Pairing in XYY Males of Drosophila melanogaster. G3 Genes|Genomes|Genetics 4: 497–
719 507.

720 Mayrose I., and M. A. Lysak, 2021 The Evolution of Chromosome Numbers: Mechanistic Models
721 and Experimental Approaches. Genome Biol. Evol. 13.
722 https://doi.org/10.1093/gbe/evaa220

723 McKee B. D., and G. H. Karpen, 1990 Drosophila ribosomal RNA genes function as an X-Y pairing
724 site during male meiosis. Cell 61: 61–72.

725 McKenna A., M. Hanna, E. Banks, A. Sivachenko, K. Cibulskis, *et al.*, 2010 The Genome Analysis
726 Toolkit: a MapReduce framework for analyzing next-generation DNA sequencing data.
727 Genome Res. 20: 1297–1303.

728 Miga K. H., Y. Newton, M. Jain, N. Altemose, H. F. Willard, *et al.*, 2014 Centromere reference
729 models for human chromosomes X and Y satellite arrays. Genome Res. 24: 697–707.

730 Mills W. K., Y. C. G. Lee, A. M. Kochendoerfer, E. M. Dunleavy, and G. H. Karpen, 2019 RNA from
731 a simple-tandem repeat is required for sperm maturation and male fertility in Drosophila
732 melanogaster. Elife 8. https://doi.org/10.7554/eLife.48940

733 Nozawa M., Y. Minakuchi, K. Satomura, S. Kondo, A. Toyoda, *et al.*, 2021 Evolutionary
734 trajectories of three independent neo-sex chromosomes in Drosophila. Cold Spring Harbor
735 Laboratory 2021.03.11.435033.

736 Paço A., F. Adega, N. Meštrović, M. Plohl, and R. Chaves, 2015 The puzzling character of
737 repetitive DNA in Phodopus genomes (Cricetidae, Rodentia). Chromosome Res. 23: 427–
738 440.

739 Petitpierre E., C. Juan, J. Pons, M. Plohl, and D. Ugarkovic, 1995 Satellite DNA and constitutive
740 heterochromatin in tenebrionid beetles, pp. 351–362 in *Kew Chromosome Conference IV.*
741 *London: Royal Botanic Gardens*,.

742 Reis M., C. P. Vieira, R. Lata, N. Posnien, and J. Vieira, 2018 Origin and Consequences of
743 Chromosomal Inversions in the virilis Group of Drosophila. Genome Biol. Evol. 10: 3152–
744 3166.

745 Schulz R., L. A. Underkoffler, J. N. Collins, and R. J. Oakey, 2006 Nondisjunction and transmission
746 ratio distortion ofChromosome 2 in a (2.8) Robertsonian translocation mouse strain.
747 Mamm. Genome 17: 239–247.

748 Shetty V., N. J. Shetty, S. R. Ananthanarayana, S. K. Jha, and R. C. Chaubey, 2017 Evaluation of
749 gamma radiation-induced DNA damage in Aedes aegypti using the comet assay. Toxicol.
750 Ind. Health 33: 930–937.

751 Stern D. L., J. Crocker, Y. Ding, N. Frankel, G. Kappes, *et al.*, 2017 Genetic and Transgenic
752 Reagents for Drosophila

753 Stewart N. B., Y. H. Ahmed-Braimah, D. G. Cerne, and B. F. McAllister, 2019 Female meiotic
754 drive preferentially segregates derived metacentric chromosomes in Drosophila. bioRxiv
755 638684.

756 Subirana J. A., M. M. Albà, and X. Messeguer, 2015 High evolutionary turnover of satellite
757 families in Caenorhabditis. BMC Evol. Biol. 15: 218.

758 Thakur J., J. Packiaraj, and S. Henikoff, 2021 Sequence, Chromatin and Evolution of Satellite
759 DNA. Int. J. Mol. Sci. 22. https://doi.org/10.3390/ijms22094309

760 Vieira C. P., A. Almeida, J. D. Dias, and J. Vieira, 2006 On the location of the gene(s) harbouring
761 the advantageous variant that maintains the X/4 fusion of Drosophila americana. Genet.
762 Res. 87: 163–174.

763 Wei K. H.-C., J. K. Grenier, D. A. Barbash, and A. G. Clark, 2014 Correlated variation and

764 population differentiation in satellite DNA abundance among lines of Drosophila
765 melanogaster. Proc. Natl. Acad. Sci. U. S. A. 111: 18793–18798.

766 Wei K. H.-C., S. E. Lower, I. V. Caldas, T. J. S. Sless, D. A. Barbash, *et al.*, 2018 Variable Rates of
767 Simple Satellite Gains across the Drosophila Phylogeny. Mol. Biol. Evol. 35: 925–941.

768 Wei K. H.-C., and D. Bachtrog, Male recombination produced multiple geographically restricted
769 neo-Y chromosome haplotypes of varying ages that correlate with onset of neo-Y decay in
770 Drosophila albomicans

771